

A CLOSER LOOK AT SPECTROGRAPHIC WAVELENGTH CALIBRATION

Marie Bøe Henriksen^{1,2}, Fred Sigernes^{1,2} and Tor Arne Johansen¹

¹ Norwegian University of Science and Technology (NTNU), Trondheim, Norway

² University Centre in Svalbard (UNIS), Longyearbyen, Norway

ABSTRACT

Methods to spectrally calibrate imaging spectrographs, also known as hyperspectral instruments, are common and known, but few look into how well the wavelength calibration performs. When building hyperspectral instruments in-house, performing sufficient wavelength calibration is necessary. This report therefore investigates how well different models describe the wavelength to pixel relationship, evaluated using Root Mean Square Error (RMSE), in a simple set-up with argon and mercury emission lines. A linear fit between pixel index and wavelength is shown to perform well, but estimating the diffraction angle with an arctan function and calculating wavelength using the grating equation also shows promising results. This report is meant to aid others calibrating their own hyperspectral imagers with limited resources by showing how wavelength calibration accuracy varies with different models.

Index Terms— Hyperspectral imager, wavelength calibration, calibration accuracy

1. INTRODUCTION

Hyperspectral imaging, or imaging spectroscopy, is a quickly growing field. Existing instruments range from large and specialized space instruments such as Medium Resolution Imaging Spectrometer (MERIS) onboard Envisat [1], to commercial instruments from companies such as Norsk Elektro Optikk (NEO) and Specim, to small and low-cost instruments that can be built in-house, e.g. [2, 3, 4]. Commercial instruments are typically calibrated before being delivered to the customer. When building the instrument in-house, however, one must also perform the calibration and make sure that it is accurate, allowing pixels on the detector to be mapped to their corresponding wavelength.

Wavelength calibration, also known as spectral calibration, determines the relationship between spectral pixel index and wavelength, so that pixels on the detector can be mapped to their corresponding wavelength. Knowledge of this pixel

The Research Council of Norway is acknowledged for funding through AMOS (grant number 223254) and the IKTPLUSS project MASSIVE (grant number 270959), and the Norwegian Space Agency and the European Space Agency acknowledged for funding through PRODEX (no. 4000132515).

to wavelength function is important as even minor spectral deviations can affect the detection of spectral features significantly [5]. Laboratory techniques to accomplish wavelength calibration includes calibration using spectral lamps, monochromator, tunable laser or gas cells [6]. Monochromator and tunable laser require more expensive and complex equipment, while the use of spectral lamps is a simpler option, especially for a wider spectral range such as the whole visible spectrum.

Often, a close to linear relation between the spectral pixel index and wavelength is expected. For instruments with a grating, the light is dispersed following the grating equation

$$m\lambda = d(\sin \alpha + \sin \beta), \quad (1)$$

where m is the spectral order, λ is the wavelength, d is the grating groove spacing, α is the angle of the incoming light (incident angle) and β is the angle of the diffracted light (diffraction angle) [7]. The change in β with wavelength is typically small, which leads to a close to linear relationship. However, small deviations from a linear fit are often observed. Solving for the diffraction angle as a function of wavelength, $\beta(\lambda)$, shows that the relationship follows an arcsin function

$$\beta(\lambda) = \arcsin \left(\frac{m\lambda}{d} - \sin \alpha \right), \quad (2)$$

which indeed can be approximated as linear in areas close to zero, but is not truly linear.

Other factors may also affect deviations from a linear fit. Chrien et al. mention that small misalignment in the angular positioning of the grating may introduce deviations [8]. Optical aberrations from the lenses may also affect the incident angles of light rays onto the grating, which again may lead to a nonlinear relation in dispersion of light.

In this report a pushbroom Hyperspectral Imager (HSI) with a transmission grating design is used in combination with argon and mercury spectral lamps to investigate the pixel to wavelength relationship. Different models are used to estimate this relationship, and their accuracy compared using Root Mean Square Error (RMSE). These investigations are meant to aid others that are developing and calibrating hyperspectral instruments in-house with little or no experience

with wavelength calibration. Understanding which parameters that are important to consider will help to minimize the wavelength calibration errors when using simple set-ups and methods.

2. EQUIPMENT

The pushbroom hyperspectral instrument presented in [3], with a transmission grating design, is used. The designed spectral range was set to 400 to 800 nm, but the full sensor covers about 240 to 970 nm. The designed center wavelength is $\lambda_c = 600$ nm, which gives a diffraction angle of $\beta_c = 10.37^\circ$. Little signal is recorded below 400 nm due to low Quantum Efficiency (QE) in the sensor, and the signal above 800 nm is normally not used due to appearance of second order diffraction effects [3]. The full spectral range can, however, be used for wavelength calibration. Specifications of the instrument are summarized in Table 1.

Table 1: Specifications of the HSI.

Parameter	Specification
Camera sensor	Sony IMX174
Image size	(1936, 1216) pixels
Designed spectral range	400 - 800 nm
Theoretical FWHM	3.3 nm
Spectral sampling distance	0.38 nm per pixel
Grating	300 lines/mm, transmission
Slit height	7 mm
Slit width	50 μm

Emission lines from argon (Ar) and mercury-argon (Hg) wavelength calibration lamps (Newport Models 6030 and 6035, respectively) were used in combination with a 30 cm integrating sphere (Model ISS-30-VA, Gigahertz Optik) with a 10 cm output port, for uniform illumination.

The theoretical Full Width at Half Maximum (FWHM) of the HSI is 3.3 nm, while the measured value tends to fall between 3.5 to 4.5 nm for the wavelengths in the desired spectral range [9]. This means that emission lines from the calibration lamps that are close to each other (less than 3-4 nm apart) will be seen as one single line by the instrument.

3. DATA ANALYSIS

The goal of the data analysis is to detect the pixel index of each recorded emission line and map them to their respective reference wavelength. The detected pixel index and wavelength pairs are further used as input to different models to estimate a function describing the pixel index to wavelength relationship. RMSE is then calculated to determine the accuracy of fit and to provide an easy method for comparison.

3.1. Data acquisition

To collect images of the spectral calibration lamps the HSI was mounted in front of the integrating sphere, illuminated by one calibration lamp at the time. The exposure time was adjusted so that the image was well lit but not overexposed, and 10 frames taken for each calibration lamp. Combined images were made by adding images of each lamp together, as seen in Fig. 1, to provide a calibration image with both argon and mercury emission lines available.

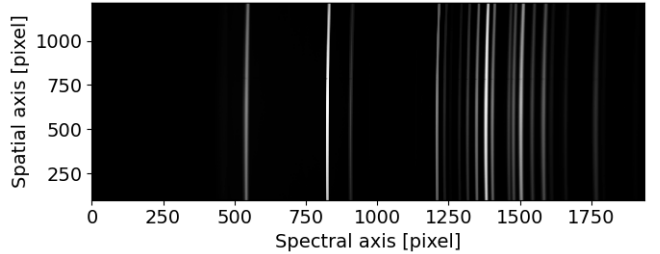


Fig. 1: Spectral calibration frame, with both argon and mercury-argon emission lines.

The center horizontal line was extracted and used for the analysis to avoid smile effects. For full calibration, the wavelength calibration can be done for each horizontal line, or smile can be corrected as in [10] or [11].

3.2. Detecting spectral lines

The center line was smoothed, and the spectral peaks detected using Python code and the `scipy.signal` function `find_peaks()`, which gives the position and height of detected peaks with peak value over a certain threshold. The detected peaks were then manually mapped to the known emission lines of argon and mercury (air wavelengths retrieved from [12] and [13]). Doing this manually makes it easy to know which detected lines are double peaks, i.e. two lines so close to each other that they are recorded as a single line within the FWHM of the instrument. Using automated detection and mapping to correct wavelengths is also possible, but it is then important to be certain that the correct wavelengths are being mapped. The detected emission lines are shown in Fig. 2, and their values in Table 2.

The detected emission lines are further divided into sets, also shown in Table 2, to investigate the impact of using double peaks and of using only a small selection of emission lines for the calibration. Set 1 contains all the detected wavelengths, set 2 is a subset with the two broadest double peaks removed, set 3 contains only single peaks (except 794.82 nm as this is partly merged with the 800.61/801.48 nm double peak), and set 4 uses only a small selection of the single peaks.

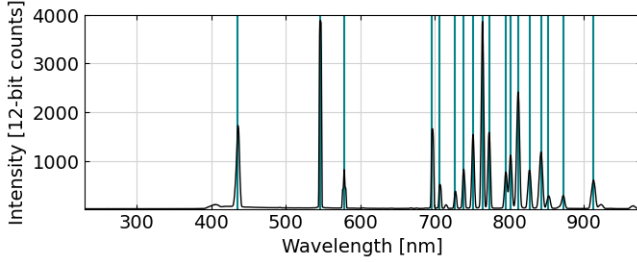


Fig. 2: Center horizontal line of the calibration frame (black line), and the reference wavelengths (blue stripes).

Table 2: Argon (Ar) and mercury (Hg) emission lines (from [12, 13]). The "x" marks emission lines used in each set.

Lamp	Peak wavelength [nm]	Set 1	Set 2	Set 3	Set 4
Hg	435.83	x	x	x	x
Hg	546.07	x	x	x	
Hg	576.96 / 579.02	x			
Ar	696.54	x	x	x	x
Ar	706.72	x	x	x	
Ar	727.29	x	x	x	
Ar	738.40	x	x	x	
Ar	750.39 / 751.46	x	x		
Ar	763.51	x	x	x	x
Ar	772.37 / 772.42	x	x		
Ar	794.82	x	x		
Ar	800.62 / 801.48	x			
Ar	810.37 / 811.53	x	x		
Ar	826.45	x	x	x	x
Ar	840.81 / 842.46	x	x		
Ar	852.14	x	x	x	x
Hg	871.68	x	x	x	
Ar	912.30	x	x	x	x

3.3. Methods

Different ways of describing the relationship between pixel index p_λ and wavelength λ are investigated to see whether using a standard polynomial curve fit is sufficient, or if including theoretical knowledge from the grating equation and/or trigonometric relations between the diffraction angle and pixel position can improve the calibration.

3.3.1. Method 1: Polynomial curve fit of λ

A second or third order polynomial fit is often used to describe the wavelength to pixel relationship [14, 8, 9]. Here, polynomial fits of different orders are used to investigate this relationship

$$\hat{\lambda} = \sum_{i=0}^n a_i \cdot p_\lambda^i, \quad (3)$$

where $\hat{\lambda}$ is the estimated wavelength, $n \in \{1..3\}$ is the order of the polynomial, p_λ the pixel index of wavelength λ , and a_i the polynomial fit coefficients.

3.3.2. Method 2: Polynomial curve fit of β

The polynomial curve fit can also be used to estimate diffraction angle (instead of wavelength) from the pixel index. The grating equation, Eq. (1), can then be used to convert from diffraction angle to wavelength. This way, the sine relation in the grating equation is excluded from the polynomial curve fit, but included in the model as the grating equation is used. The polynomial curve fit becomes

$$\hat{\beta} = \sum_{i=0}^n b_i \cdot p_\lambda^i, \quad (4)$$

where $\hat{\beta}$ is the estimated diffraction angle, and b_i are the polynomial fit coefficients. By assuming $\alpha = 0$ and using spectral order $m = 1$, the grating equation applied becomes

$$\hat{\lambda} = d \cdot \sin \hat{\beta}, \quad (5)$$

which completes the map from pixel index to wavelength.

3.3.3. Method 3: Curve fit of β with \arctan

The sensor is tilted 10.37° from the grating, matching the diffraction angle β_c of the center wavelength. According to simple trigonometry, an offset in diffraction angle, denoted $\Delta\beta = \hat{\beta} - \beta_c$, should result in an offset in pixel position on the sensor, $\Delta p_\lambda = p_\lambda - p_{\lambda_c}$, according to

$$\Delta\beta = \arctan\left(\frac{\Delta p_\lambda \cdot p_{width}}{l}\right), \quad (6)$$

where $\hat{\beta}$ is the estimated diffraction angle and p_λ the corresponding pixel index, p_{λ_c} is the pixel index of the center wavelength, p_{width} is the width of each pixel, and l is the focal length of the detector lens.

A least squares curve fit is made to the function

$$\hat{\beta} = c_0 + \arctan(c_1 + c_2 \cdot p_\lambda)), \quad (7)$$

where $c_0..c_2$ are the coefficients of the fit. From theory, c_0 corresponds to β_c . The estimated diffraction angle is again used with the simplified grating equation in Eq. (5) to find the estimated wavelength.

3.3.4. Method 4: Curve fit of λ with grating equation

In addition, a least squares curve fit is made to the grating equation, combined with the diffraction angle to pixel position relationship described in Eq. (7). The function used for the fit is

$$\hat{\lambda} = d_0 \cdot (\sin(d_1) + \sin(d_2 + \arctan(d_3 + d_4 \cdot p_\lambda))), \quad (8)$$

where $d_0..d_4$ are the coefficients of the fit. From theory, d_1 corresponds to α , while d_2 here corresponds to β_c . An additional version assuming $\alpha = 0$ was also tested by forcing $d_1 = 0$, to reduce the number of coefficients that needed to be estimated.

3.4. Leave-one-out cross-validation and RMSE

Leave-one-out cross-validation is used when testing the different models. For each set of emission lines, all lines except one are used to calculate the model coefficients. The model is then tested on the one emission line that was not included in making the model. $\hat{\lambda}$ is estimated from the pixel index p_λ . The error from the corresponding reference wavelength is calculated as $e = \lambda_{ref} - \hat{\lambda}$. This is done for every emission line in the set, resulting in a list of errors for each set.

The RMSE is further used as a measure on how well different models describe the wavelength to pixel relation. The RMSE is calculated as

$$RMSE = \sqrt{\frac{1}{m} \sum_{j=0}^m e_j^2}, \quad (9)$$

where m is the number of emission lines in the set, and e_j is the error for each emission line in the set. The RMSE is calculated for each model with each set.

4. RESULTS AND DISCUSSION

The pixel indices of the detected emission lines form a close to linear relation with the reference wavelengths, as seen in Fig. 3. This confirms the close to linear relationship that is expected and commonly assumed. There are, however, small deviations from the linear fit, as seen in Fig. 4, where a systematic error pattern appears.

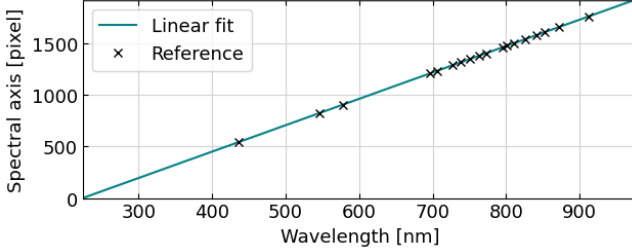


Fig. 3: Pixel index of the reference wavelengths (crosses) with a linear fit (blue line) showing close to linear relationship between reference wavelength and recorded pixel index.

The RMSE values for each method with each set are shown in Table 3. The values for the curve fits of wavelength via the grating equation (method 4) are shown in cursive as these fits depend heavily on the initial guess values of the coefficients (input parameters to the least squares curve fit

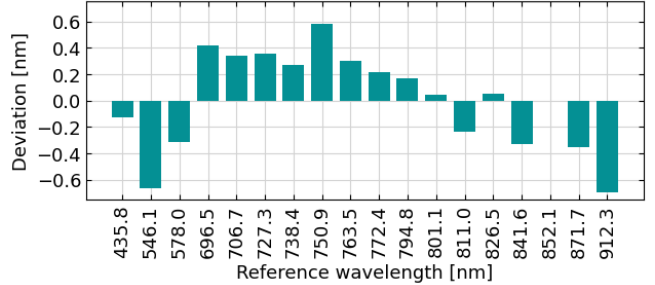


Fig. 4: Deviation between the reference wavelengths and estimated wavelength of the pixel indices after a linear fit.

Table 3: RMSE values for the different methods and sets. n is the order of polynomial fit.

Method	Set 1	Set 2	Set 3	Set 4
1	n=1	0.131	0.142	0.155
	n=2	0.180	0.191	0.231
	n=3	0.247	0.267	0.233
2	n=1	0.185	0.201	0.246
	n=2	0.156	0.168	0.203
	n=3	0.249	0.269	0.233
3		0.114	0.125	0.148
4		0.190	0.218	0.185
	$\alpha=0$	0.192	0.209	0.425
				0.786

function). This is most likely due to few measurement points, as estimating 4-5 coefficients from only 6-18 points gives large uncertainties to the resulting model.

The lowest RMSE values for all sets are found with the curve fit of diffraction angle (method 3). This suggests that including theoretical models such as the grating equation and simple trigonometry can help to explain the pixel to wavelength relationship better than a standard linear fit. The first order polynomial curve fit of wavelength (method 1 with $n = 1$, corresponds to linear fit) also shows low RMSE values for all sets, suggesting that a linear fit still is a good approximation even though small deviations can be seen.

For most methods, set 1 has lowest RMSE values, and the values increase as the number of emission lines in the sets decrease. This suggests that there are too few measurement points (emission lines) to make good fits. The double peaks does not seem to degrade the results, but rather improve the accuracy, which might be different if more points were available.

The deviation between reference wavelengths and estimated wavelengths (as shown for method 1 with $n = 1$ in Fig. 4) was plotted for the different methods and sets (not shown). For all methods and sets the highest deviations were found for the shortest wavelengths. Most reference wavelengths are located in the upper part of the spectrum investigated, as seen in Fig. 2, leaving the lower part of the spectrum

thin with measurement points. Lamps providing additional emission lines in the lower part of the spectrum might therefore help to improve all methods.

The pixel to wavelength relationship can be hard to model as aberrations from the lenses and other optical effects may alter the paths of the light rays. Errors from the calibration equipment or from the pre-processing such as the peak detection algorithm may also affect the results.

5. CONCLUSIONS AND FUTURE WORK

The RMSE values in Table 3 generally show no clear trends to which model is the better choice, but confirms that the pixel to wavelength relationship is mainly linear and that a linear fit might be sufficient. More measurement points are needed, specially in the lower part of the spectrum (400 to 600 nm) to improve the models further.

Future work will therefore be to using different calibration methods or additional spectral lamps to achieve more measurement points across the full spectrum of interest. Different ways of detecting the emission line peaks in the pre-processing can also be tested.

6. REFERENCES

- [1] M. Rast, J. L. Bézy, and S. Bruzzi, “The ESA Medium Resolution Imaging Spectrometer MERIS a review of the instrument and its mission,” *International Journal of Remote Sensing*, vol. 20, no. 9, pp. 1681–1702, 1999.
- [2] F. Sigernes, M. Syrjäsuo, R. Storvold, J. Fortuna, M. E. Grøtte, and T. A. Johansen, “Do it yourself hyperspectral imager for handheld to airborne operations,” *Optics Express*, vol. 26, no. 5, pp. 6021–6035, 2018.
- [3] M. B. Henriksen, E. F. Prentice, C. M. van Hazendonk, F. Sigernes, and T. A. Johansen, “Do-it-yourself VIS/NIR pushbroom hyperspectral imager with C-mount optics,” *Optics Continuum*, vol. 1, no. 2, pp. 427, 2022.
- [4] H. Saari, V.-V. Aalos, A. Akujärvi, T. Antila, C. Holmlund, U. Kantojärvi, J. Mäkinen, and J. Ollila, “Novel miniaturized hyperspectral sensor for UAV and space applications,” in *Proc. SPIE 7474, Sensors, Systems, and Next-Generation Satellites XIII, 74741M*, 2009.
- [5] R. O. Green, “Spectral calibration requirement for Earth-looking imaging spectrometers in the solar-reflected spectrum,” *Applied Optics*, vol. 37, no. 4, pp. 683–690, 1998.
- [6] X. Yu, Y. Sun, A. Fang, W. Qi, and C. Liu, “Laboratory Spectral Calibration and Radiometric Calibration of Hyper-spectral Imaging Spectrometer,” in *ICSAI: 2nd International Conference on Systems and Informatics, ICSAI 2014*, 2015, pp. 871–875.
- [7] C. Palmer and E. Loewen, *Diffraction Grating Handbook*, Newport Corporation, 7 edition, 2014.
- [8] T. G. Chrien, R. O. Green, and M. L. Eastwood, “Accuracy of the spectral and radiometric laboratory calibration of the Airborne Visible/Infrared Imaging Spectrometer,” in *Proc. SPIE 1298, Imaging Spectroscopy of the Terrestrial Environment*, 1990.
- [9] M. B. Henriksen, E. F. Prentice, T. A. Johansen, and F. Sigernes, “Pre-Launch Calibration of the HYPSO-1 Cubesat Hyperspectral Imager,” in *IEEE Aerospace Conference*, 2022.
- [10] K. A. Riihiaho, M. A. Eskelin, and I. Pöölönen, “A do-it-yourself hyperspectral imager brought to practice with open-source python,” *Sensors*, vol. 21, no. 1072, 2021.
- [11] M. B. Henriksen, J. L. Garrett, E. F. Prentice, A. Stahl, and T. A. Johansen, “Real-time corrections for a low-cost hyperspectral instrument,” in *10th Workshop on Hyperspectral Image and Signal Processing, Evolution in Remote Sensing (WHISPERS)*, 2019.
- [12] National Institute of Standards and Technology (NIST), “Strong lines of argon (ar),” Retrieved from <https://www.physics.nist.gov/PhysRefData/Handbook/Tables/argontable2.htm>.
- [13] National Institute of Standards and Technology (NIST), “Strong lines of mercury (hg),” Retrieved from <https://www.physics.nist.gov/PhysRefData/Handbook/Tables/mercurytable2.htm>.
- [14] S. Delwart, L. Bourg, R. Preusker, and R. Santer, “MERIS spectral calibration campaigns,” *Sensors, Systems, and Next-Generation Satellites VIII*, vol. 5570, no. November 2004, pp. 381, 2004.